

FULL PAPER

Open Access



Frictional strength of North Anatolian fault in eastern Marmara region

Ali Pinar* , Zeynep Coşkun, Aydın Mert and Doğan Kalafat

Abstract

Frequency distribution of azimuth and plunges of P - and T -axes of focal mechanisms is compared with the orientation of maximum compressive stress axis for investigating the frictional strength of three fault segments of North Anatolian fault (NAF) in eastern Marmara Sea, namely Princes' Islands, Yalova–Çınarcık and Yalova–Hersek fault segments. In this frame, we retrieved 25 CMT solutions of events in Çınarcık basin and derived a local stress tensor incorporating 30 focal mechanisms determined by other researches. As for the Yalova–Çınarcık and Yalova–Hersek fault segments, we constructed the frequency distribution of P - and T -axes utilizing 111 and 68 events, respectively, to correlate the geometry of the principle stress axes and fault orientations. The analysis yields low frictional strength for the Princes' Island fault segments and high frictional strength for Yalova–Çınarcık, Yalova–Hersek segments. The local stress tensor derived from the inversion of P - and T -axes of the fault plane solutions of Çınarcık basin events portrays nearly horizontal maximum compressive stress axis oriented N154E which is almost parallel to the peak of the frequency distribution of the azimuth of the P -axes. The fitting of the observed and calculated frequency distributions is attained for a low frictional coefficient which is about $\mu \approx 0.1$. Evidences on the weakness of NAF segments in eastern Marmara Sea region are revealed by other geophysical observations. Our results also show that the local stress field in Çınarcık basin is rotated $\approx 30^\circ$ clockwise compared to the regional stress tensor in Marmara region derived from the large earthquakes, whereas the local stress tensor in Yalova–Çınarcık area is found to be rotated $\approx 30^\circ$ counterclockwise. The rotation of the two local stress fields is derived in the area where NAF bifurcates into two branches overlaying large electrical conductor.

Keywords: Local stress field, Frictional coefficient, Marmara Sea, Çınarcık basin, Stress field rotation

Background

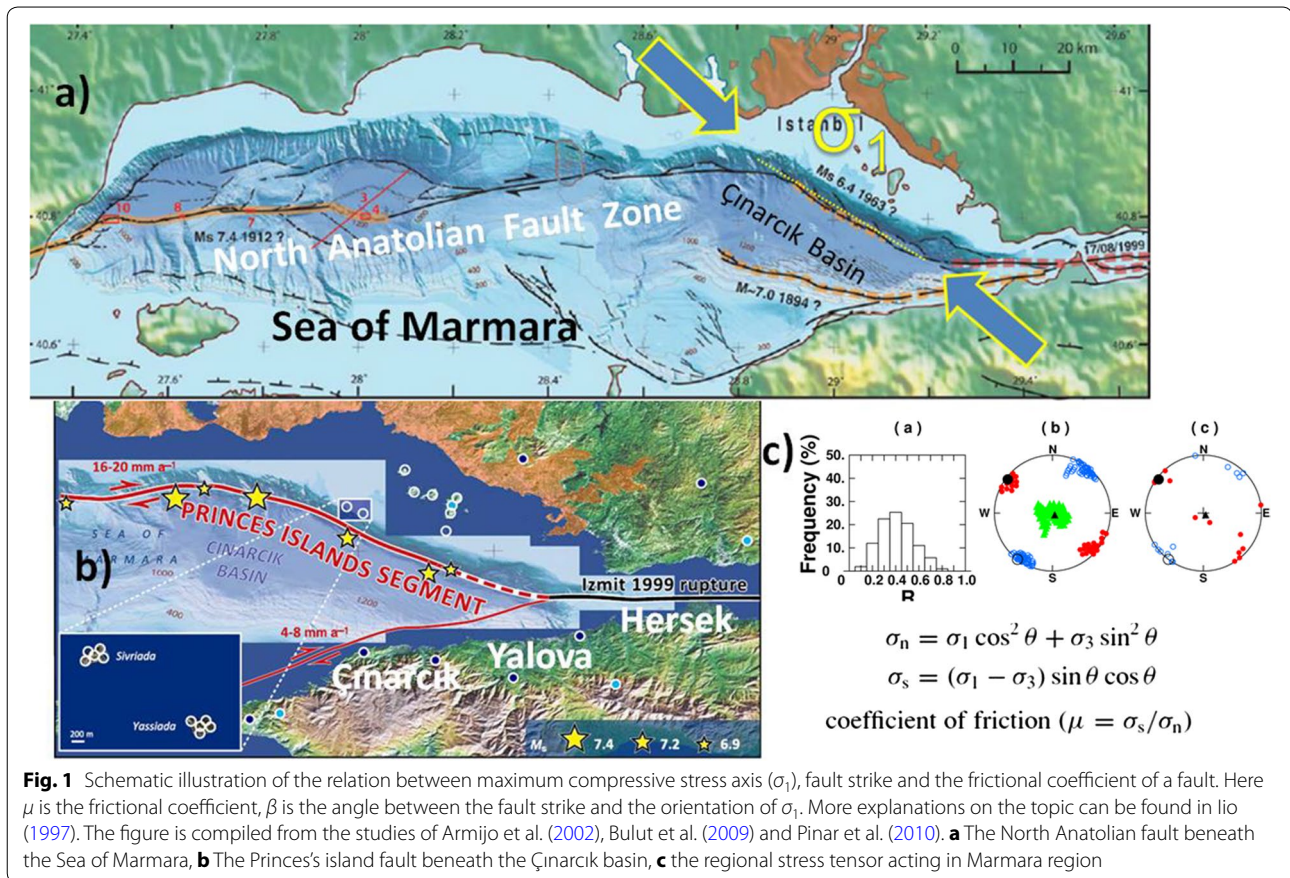
The regional stress field along with the local stress perturbations provides invaluable information to understand the seismic hazard of a region under investigation and help to localize the sources of the tectonic driving forces (Stefanik and Jurdy 1992). In such studies, earthquake focal mechanisms and microtectonic field observations are widely used to retrieve the stress tensor parameters (Zoback 1993; Pinar et al. 2003, 2010; Över et al. 2013). On the other hand, the Coulomb failure criteria point out that the orientation of the maximum compressive stress axis and the strike of the potentially active faults are interconnected through the frictional coefficient of

faults (King et al. 1994; Iio 1997). Thus, the orientation of the active faults in a region along with the stress data can be applied as constraints in seismotectonic zonation (Zoback 1993).

The stress field acting in Marmara Sea region was the subject of several studies in the past resulting in a consensus with NW–SE trending maximum compressive principal stress axis (σ_1) where strike-slip tectonic regime dominates (Gürbüz et al. 2000; Kiratzi 2002; Pinar et al. 2003, 2010; Örgülü 2011). The orientation of σ_1 axis obtained by those researches is more or less in parallel with the strike of the Princes' Islands fault segment of the NAFZ in eastern Marmara Sea (Fig. 1a, b).

The stress tensor inversion results portrayed in Fig. 1c point out a stress tensor, with azimuth and plunge values of $\sigma_1 = (307, 4)$, $\sigma_2 = (91, 86)$ and $\sigma_3 = (217, 0)$ using focal mechanisms of earthquakes in Marmara region during

*Correspondence: pinara@boun.edu.tr
Kandilli Observatory and Earthquake Research Institute, Bogazici University, Istanbul, Turkey



the last century. The Princes' Islands fault orientation within such stress field in Marmara region mimics a low coefficient of friction. One may come to such conclusion considering the basic relation between the orientation of the maximum and minimum principal stress axes, the shear and normal stresses, and the orientation of a fault defined in the relations of σ_n and σ_s given in Fig. 1c, where σ_s and σ_n are the shear and normal stresses, respectively, acting on a fault plane, and θ is the angle between the fault normal and maximum compressive stress axis (Twiss and Moores 1992, pp. 154). According to these relations, when the trend of σ_1 axis is close to the strike of the fault, i.e., θ is close to 90° , the shear stress acting on the fault plane approaches zero. On the other hand, the ratio between the shear and normal stresses acting on a fault plane is proportional to the coefficient of friction ($\mu = \sigma_s/\sigma_n$) of that fault plane (Twiss and Moores 1992, pp. 211) when the fault slips. Based on such knowledge, the fault parallel trend of σ_1 axis (fault normal trend of σ_3 axis) suggests a low coefficient of friction. Similarly, when the trend of σ_1 axis is perpendicular to the strike of fault, i.e., θ is close to 0° , the shear stress acting on fault plane and the coefficient of friction approach zero (Pinar et al. 2010).

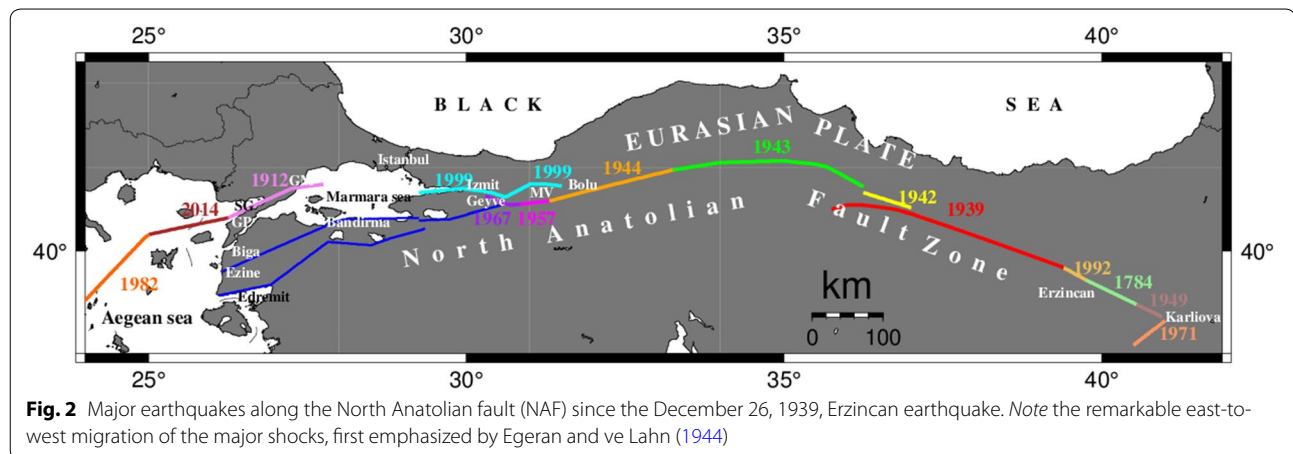
The NAFZ splits into two branches as it extends from the Gulf of İzmit toward the Çınarcık basin (Fig. 1). The NW–SE extending branch is called Princes Islands fault segment, the WSE–ENE extending branch is called Yalova–Çınarcık segment, and the third segment is extending between Hersek and Yalova (Fig. 1b).

The objective of this study is to investigate the local stress tensor acting around these three fault segments of NAFZ in eastern Marmara Sea region with an aim to retrieve information on the strength of those faults. Special attention is paid to the Princes' Island fault segment which is parallel to the maximum compressive stress axis (σ_1) of the regional stress tensor acting in Marmara region.

Tectonic setting

The North Anatolian fault zone (NAFZ)

The North Anatolian fault (NAF) is one of the largest currently active dextral strike-slip fault forming the plate boundary between Eurasia and Anatolia. NAF extends over 1600 km between Karlıova triple junction, where it meets the sinistral East Anatolian fault, to the Gulf of Saros in the northern Aegean Sea, where extensional regime dominated extends further west to mainland Greece. Between 1939 and 1999 (Fig. 2), the NAF



ruptured in a sequence of large earthquakes ($M > 7$) initiated by 1939 M_w 7.9 Erzincan earthquake and propagated westward over 1000 km (Toksöz et al. 1979; Stein et al. 1997; Reilinger et al. 2000; Şengör et al., 2005) and August 17, 1999, M_w 7.6 İzmit earthquake ruptured a 150-km-long segment of the NAF (Barka 2002). The NAF was recognized as a major strike-slip fault by Ketin (1948), and numerous geological, geomorphological and geophysical studies have been carried out, especially after two recent catastrophic earthquakes of August 17, 1999, and November 12, 1999 (Şengör et al. 2005).

Ketin (1948) noted that surface breaks of all major earthquakes in northern Turkey since 1939 had generally east–west striking right-lateral fault character and the vertical component of the motion always upthrew the southern block (Şengör et al. 2005). Combining these observations with previously known information about the North Anatolian earthquake belt, he declared that the seismic source in northern Turkey was the product of a major, active, dextral strike-slip fault and after Yenice–Gönen earthquake (Ketin and Rösli 1953) and he pointed out that the fault continued south of the Sea of Marmara (Şengör et al. 2005).

The NAFZ in the Marmara Sea

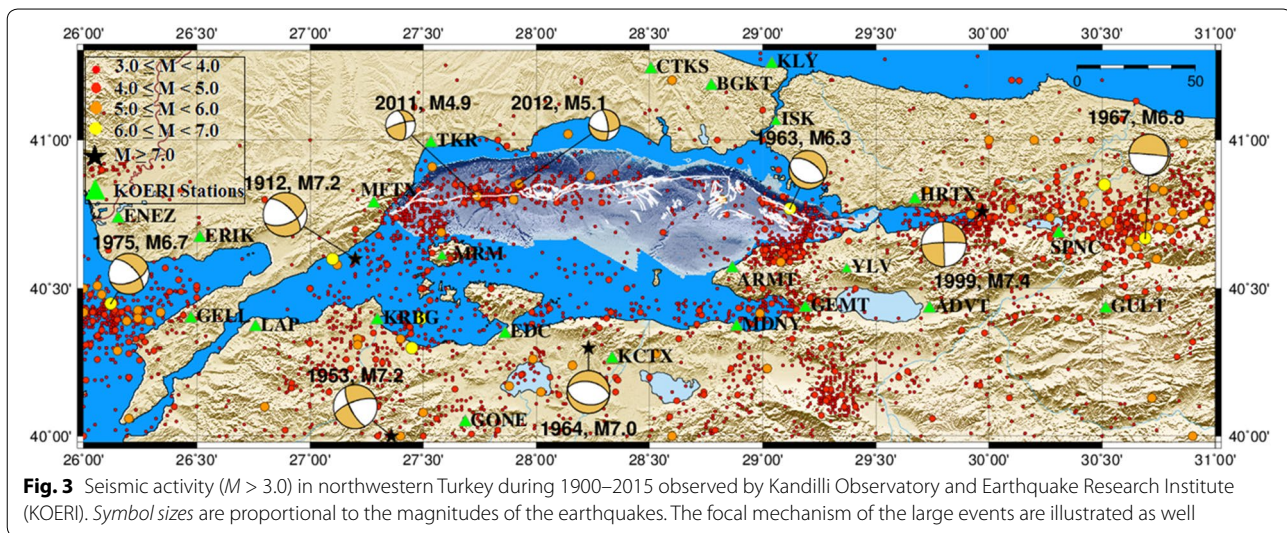
Ketin (1968) suggested the probability of east–west striking rift underlay the northern trough of the Sea of Marmara. Likewise, Pinar (1943) also suggested the presence of east–west striking trough in the northern part of the sea. This suggestion was followed by McKenzie (1972) who pointed out that the Sea of Marmara is under east–west striking extensional regime which is northeast–southwest directed (Şengör et al. 2005). Following the M_w 7.4 1999 Kocaeli earthquake Le Pichon et al. (2001) obtained for the first time detailed bathymetric and high-resolution seismic reflection data. The results of

the study have shown that a single, throughgoing dextral strike-slip fault, Main Marmara Fault connects the Gulf of İzmit fault to the east with the Ganos fault to the west (Le Pichon et al. 2003)

The Marmara Sea is located in a transition region where the dextral strike-slip regime of the NAF to the east meets the extensional regime of the Aegean Sea to the west (Fig. 2) and splits into two main branches as northern NAF and southern NAF (Gürbüz et al. 2000).

The Sea of Marmara is a marine basin located south of İstanbul, about 230 km long and 70 km wide with a shallow shelf to the south (Ambraseys 2002). The northern part comprises three subbasins with up to 1250 m water depth, namely from west to east the Tekirdağ, Central and Çınarcık basins, and separated by topographic highs, the Western and Central highs. Due to the depths and bathymetric gradients of the Tekirdağ and Çınarcık basins, high local seismic activity (Fig. 3) is observed in those subbasins (Smith et al. 1995; Wong et al. 1995; Parke et al. 1999; Okay et al. 2000; Bulut et al. 2009; Örgülü 2011).

Especially after İzmit earthquake, several marine-based international studies have been carried out in order to have better knowledge about the structure of the Marmara Sea. The main common result of the studies carried out by Le Pichon et al. (1999, 2000), Rangin et al. (2001, 2004), İmren et al. (2001), Le Pichon et al. (2001, 2003), Demirbağ et al. (2003), Armijo et al. (2002, 2005), Sato et al. (2004), Carton (2005), Carton et al. (2007), Laigle et al. (2008) and Becel et al. (2009) indicates the presence of a westward-propagating single dextral strike-slip fault model acting in the northern branch of the Marmara Sea and comprises three subbasins, namely from east-to-west Çınarcık, Central and Tekirdağ basins. On the contrary to the single dextral strike-slip fault model, Armijo et al. (1999, 2002, 2005), Carton (2005) and Carton et al. (2007)



suggested a pull-apart model that considers a segmented fault system that interconnects three basins in the northern Marmara Sea. The model suggested by the authors pointed out that normal faults bound the margins of these basins and indicate that such a configuration forming at a step-over between two strike-slip fault segments requires subsidence and localized crustal stretching that can be responsible for structural evolution of deep basins in the Marmara Sea (Örgülü 2011).

The Çınarcık basin

The Çınarcık basin is the largest and the deepest basin in the Marmara Sea (Gazioğlu et al. 2002). The basin is a wedge-shaped basin oriented N110°E, about 50 km long and up to 15–18 km wide, with up to of 1270 m seafloor depth. The basin is bounded by large topographic escarpments on its north and south sides and by a topographic high to the west which isolates it from the Central Basin. On the east, where it meets the Gulf of İzmit, the basin considerably narrows (Carton et al. 2007). Various alternative models are considered for the development of the Çınarcık basin. Armijo et al. (2002), Carton (2005) and Carton et al. (2007) pointed out that the opening of the basin is driven due to a pull-apart model. A trans-tensional model was also proposed by Laigle et al. (2008) and Becel et al. (2009). Marine-based seismic reflection studies of İmren et al. (2001), Le Pichon et al. (2001, 2003) and Demirbağ et al. (2003) and focal mechanism studies by Örgülü and Aktar (2001) and Özalaybey et al. (2002) indicate the presence of a dextral strike-slip fault along the northeastern margin of the basin (Örgülü 2011).

The largest event in the instrumental period occurred in September 18, 1963, $M_w = 6.3$ is thought to have broken part of the northeastern Çınarcık basin with an

epicentral location of 29°12'E, 40°54'N (Taymaz et al. 1991). Armijo et al. (2005) observed a small fresh break 20–30 km long along the NE Çınarcık basin fault, which might correspond to the 1963 earthquake rupture (Carton et al. 2007).

The microseismicity studies carried out in the region, especially the aftershocks of the 1999 İzmit earthquake, indicate mixed focal mechanisms in Çınarcık basin such as strike-slip, extensional and oblique-slip (Özalaybey et al. 2002; Karabulut et al. 2002; Sato et al. 2004). Le Pichon et al. (2001) and İmren et al. (2001) proposed that the northern segment is a single strike-slip fault cutting across the Sea of Marmara, and on the other hand, Armijo et al. (2002) suggested that the Çınarcık basin was surrounded by normal and strike-slip faults (Bulut et al. 2009). By using a dense grid of multichannel seismic reflection profiles, Carton et al. (2007) provide seismic images of a nearly three-dimensional view of the structure of the basin. The results of this study suggest that the basin has a non-uniformly distributed thick sediment fill with a maximum sediment thickness of 6 km or more. It is pointed out that along both northern and southern margins of the basin, deep penetrating basin-bounding faults with extensional component of motion are imaged instead of single throughgoing strike-slip fault, neither a cross-basin nor a pure strike-slip fault existing along the northern margin (Carton et al. 2007). Bulut et al. (2009) observed microearthquakes in and around the Çınarcık basin. The resulting fault plane solutions of their study shows that strike-slip mechanism is dominant along the northern slope of the basin and toward the western end of the basin a substantial thrust component on either NE–SW or NW–SE trending fault planes. Moreover, the distribution of hypocenters provides an indication of a

complex nature of faults beneath the basin rather than a single fault zone running through (Bulut et al. 2009). Based on seismicity, focal mechanism and stress data, Örgülü (2011) also infers that the present day deformation in the Marmara Sea is mainly driven by a dextral strike-slip regime in both northern and southern splays of NAF and also normal and thrust faulting regime that represents shallow processes at local scales.

Data and method

In this study, we use focal mechanism data sets and apply analysis methods to infer information on the frictional coefficient of faults. Also, we analyzed broadband waveform data and obtained 25 CMT inversions of $M > 3$ events occurred in eastern Marmara Sea located mostly in Çınarcık basin area. For CMT analysis, we used the method given in Kuge (2003). Including 18 focal mechanisms of smaller events determined by Bulut et al. (2009) and 12 CMT solutions of Pinar et al. (2003) in total, we utilize 55 events to derive a stress tensor acting in Çınarcık basin area with the aim to understand the strength of the faults occurring there. As for the Yalova–Çınarcık and Yalova–Hersek fault segments, we utilize 111 and 68 focal mechanisms of events obtained by Pinar et al. (2010).

Relation between the geometry of σ_1 and fault orientation

For estimation of the coefficient of friction of faults, we use the method given in Iio (1997). According to Coulomb failure criteria, the orientation of the maximum compressive stress axis and the strike of the potentially active faults are interconnected through frictional coefficient. The maximum Coulomb failure stress attains a maximum value when $\beta = 1/2 \arctan(1/\mu)$, where β is the angle between the direction of the maximum compression and the fault plane orientation (Fig. 4). Thus, the orientation of the fault plane relative to the maximum compression direction is determined by the value of the coefficient of friction (Iio 1997). In the following paragraphs, the relation between β and μ is illustrated and the formulation is shown

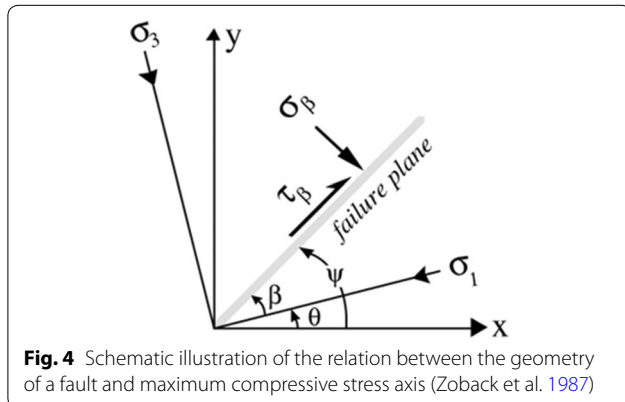


Fig. 4 Schematic illustration of the relation between the geometry of a fault and maximum compressive stress axis (Zoback et al. 1987)

$$\sigma_\beta = \sigma_1 \cos^2 \beta + \sigma_3 \sin^2 \beta \quad (1)$$

$$\tau_\beta = (\sigma_1 - \sigma_3) \cos \beta \sin \beta \quad (2)$$

where τ_β = shear stress and σ_β = normal stress. The relation between the strike of a fault and azimuth of σ_1 is summarized in King et al. (1994) as follows;

$$\sigma_f = \tau_\beta - \mu(\sigma_\beta - p) \quad (3)$$

where σ_f = Coulomb failure stress, μ = frictional coefficient, p = pore pressure.

$$\sigma_\beta = 0.5(\sigma_1 + \sigma_3) - 0.5(\sigma_1 - \sigma_3) \cos 2\beta \quad (4)$$

$$\tau_\beta = 0.5(\sigma_1 - \sigma_3) \sin 2\beta \quad (5)$$

$$\sigma_f = 0.5(\sigma_1 - \sigma_3)(\sin 2\beta - \mu \cos 2\beta) - 0.5\mu(\sigma_1 + \sigma_3) + \mu p \quad (6)$$

The derivative of Coulomb failure stress with respect to the angle between the faults and the maximum compression direction yields the required relation between frictional strength and geometry of the faults and maximum compressive stress axis as given below.

$$d\sigma_f/d\beta \rightarrow \tan 2\beta = 1/\mu \rightarrow \beta = 0.5 \arctan(1/\mu)$$

By virtue of the fact that, the P -axis of focal mechanisms has an angle of 45° from the fault plane, the direction of the P -axis does not coincide with the direction of the maximum compressional stress when values of μ are large (Iio 1997). Figure 5 schematically illustrates the relation between the P -axis azimuth and the maximum compression when μ is set to 0.6.

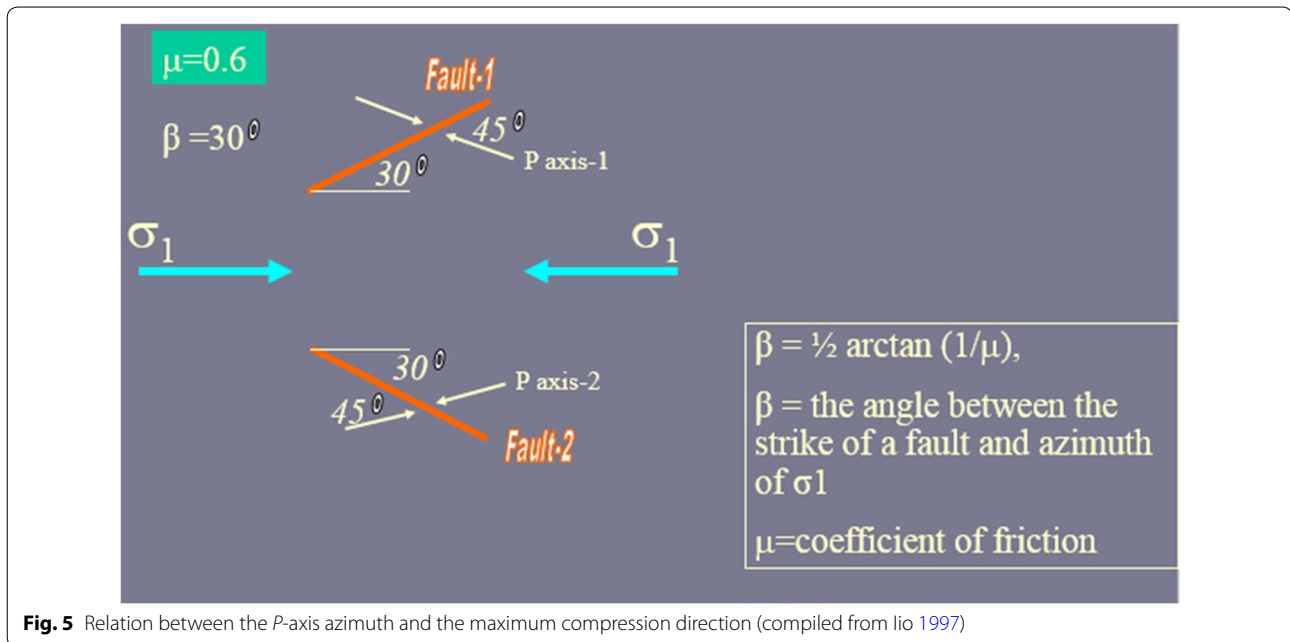
As explained in Iio (1997), the coefficient of friction on faults can be inferred from the frequency distribution of the P -axis azimuths. For large values of μ it is shown that the frequency distribution of the P -axis has two peaks far from the azimuth of the maximum compression, while for smaller values of μ the peak of the distribution is close to the azimuth of the maximum compression.

Using the β equation, in the following we show how the difference between the azimuths of P -axis (P) and maximum compressive stress (σ_1) direction is related with the frictional coefficient (μ).

$$\begin{aligned} m = 0.0 &\rightarrow \beta = 45 (P - s_1 = 0) \\ m = 0.1 &\rightarrow \beta = 42 (P - s_1 = \pm 3) \\ m = 0.3 &\rightarrow \beta = 37 (P - s_1 = \pm 8) \\ m = 0.5 &\rightarrow \beta = 32 (P - s_1 = \pm 13) \\ m = 0.7 &\rightarrow \beta = 28 (P - s_1 = \pm 17) \end{aligned}$$

CMT inversion for eastern Marmara Sea events

The earthquakes we used were recorded on several broadband seismic stations in Marmara region operated by Kandilli Observatory and Earthquake Research



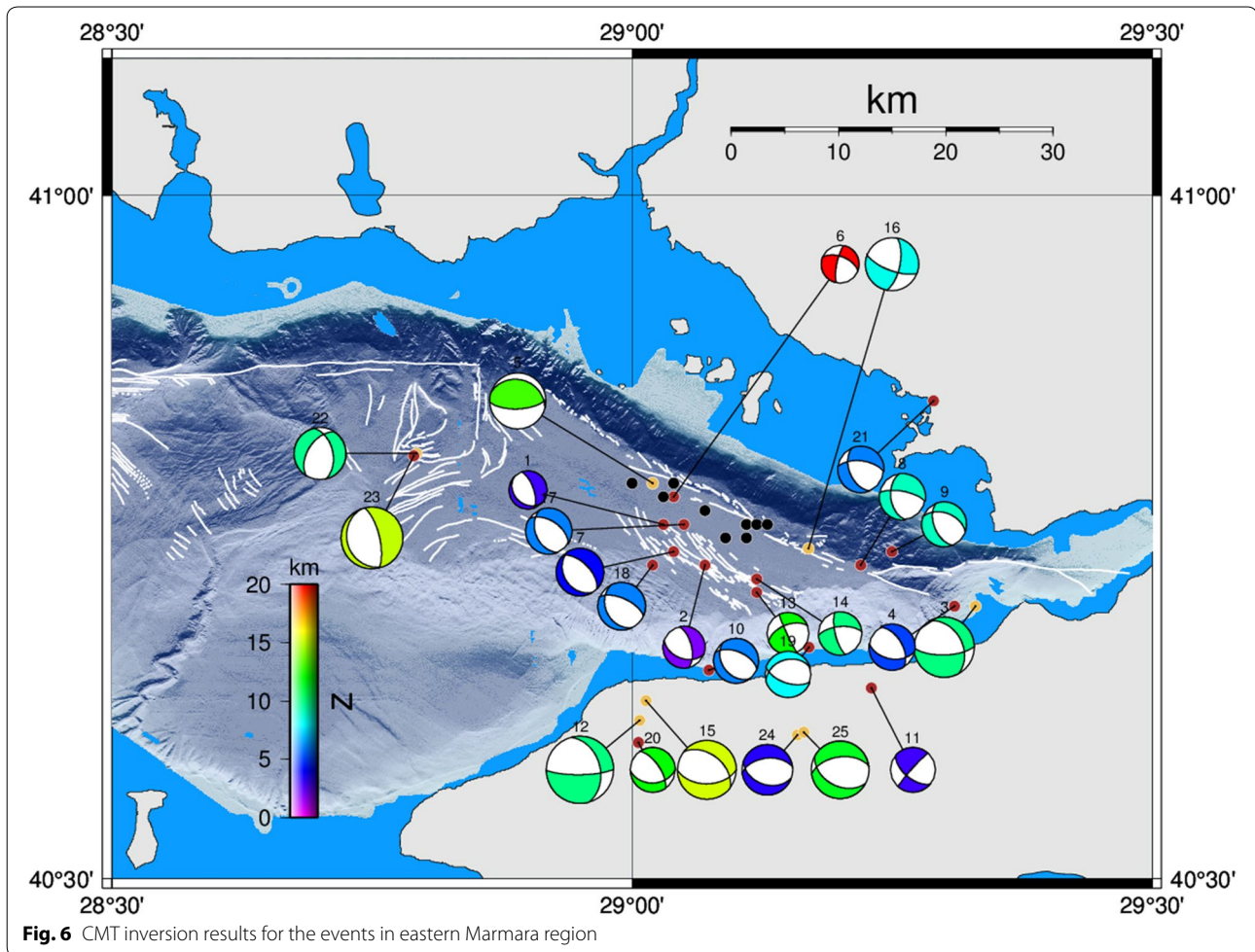
Institute (KOERI) providing good azimuthal coverage (www.koeri.boun.edu.tr) to retrieve source parameters for the Çınarcık basin earthquakes (Fig. 6). The waveform modeling methodology developed by Kuge (2003) that models displacement seismograms at one or more stations at local distances was applied. A centroid location is determined by a 3D-grid search scheme that achieves the best fit between observed and synthetic displacement seismograms. The synthetics are calculated following Kohketsu (1985) for a horizontally layered velocity structure. We calculated Green's functions using the KOERI crustal structure model developed by Kalafat et al. (1987) used routinely for earthquake locations in the region. By comparing the observed arrival times for P - and S -waves to the predicted ones, we confirmed that this velocity model provides a good fit to the observed P and S travel times.

Our data were band-pass-filtered between 0.04 and 0.1 Hz during the inversion process, and a uniform weight was assigned to all the seismograms. The goodness of fit between observed and predicted seismograms for the two models is evaluated using the variance reduction (VR) (Kuge, 2003). The larger the value of VR, the better the fit. The maximum value of VR is 100. The variance reduction is calculated for various depths, and we select the faulting mechanism in which the VR is the maximum. The results of the moment tensor inversion for all the events analyzed are illustrated in Fig. 6 and Table 1.

Stress tensor inversion

The stress tensor inversion method we use is described in Gephart (1990). We follow the same approach that was used to derive stress tensor from the focal mechanisms of the events in Marmara region by Pinar et al. (2003). Our data are the orientation of the P - and T -axes of the fault plane solutions we determined. In the method, the earthquakes are assumed to have occurred in a region with no spatial or temporal changes in the stress field, and the associated slip direction is the shear stress direction on the fault plane. The method yields a stress tensor defined by the three principal stress components, namely maximum compression, (σ_1), intermediate compression, (σ_2), minimum compression, (σ_3), and the stress magnitude ratio defined as $R = (\sigma_2 - \sigma_1)/(\sigma_3 - \sigma_1)$. The value of R is an indicator of the dominant stress regime acting in the region under investigation. The combination of these four parameters (σ_1 , σ_2 , σ_3 and R) is called a stress model, and the model that most closely matches the whole observed data set is called the best-fitting stress model. The best-fitting model is searched for in a grid over the four model parameters, systematically adjusting one at a time through a wide range of possibilities (Gephart 1990). The measure of misfit is given by the smallest rotation about an axis of any orientation that brings one of the nodal planes and its slip direction into an orientation consistent with the stress model.

The results of the stress tensor inversion using the focal mechanisms given in Figs. 6 and 7 are illustrated in Fig. 8. For more explanation, see the caption of Fig. 8.



Fault strength results

Frequency distribution of the azimuths of P -axes in Çınarcık basin area

Using the focal mechanisms for the Çınarcık basin events obtained in this study along with the fault plane solutions by Pinar et al. (2003) and Bulut et al. (2009), totally 55 focal mechanisms were used to derive a stress tensor acting in Çınarcık basin area (Fig. 8). The best stress tensor results point out a nearly horizontal maximum compressive stress axis with an azimuth of 154° from the north.

As described in “Relation between the geometry of σ_1 and fault orientation” section, the difference between the azimuths of the maximum compressive stress axis σ_1 and the strike of the fault plane carries information on the frictional strength of the faults. In this frame, firstly a stress tensor inversion of using the focal mechanisms was carried out to derive the orientation of σ_1 in Çınarcık basin which was determined as $N154^\circ E$. In the next step, a population of β angles between the fault strikes and σ_1 needs to be determined. However, it is quite challenging to distinguish the fault plane from the two nodal planes,

especially for the small size events. Therefore, it is not an easy task to measure directly the angle between σ_1 and the fault plane. For these reasons, we adopt the assumptions made by Iio (1997) where he analyzed the distribution of P -axis azimuths instead of directly analyzing the β angles, assuming that the average direction of P -axes is the direction of the maximum compressional stress and that directions of fault planes are calculated from those of P -axes.

Considering the fact that the P -axes are at an angle of 45° from the fault orientations analyzing directly the difference between the azimuth of σ_1 and frequency distribution of P -axis could be an approximation of investigating the average β angle. Thus, assuming that the population of the P -axis reflects the population of the fault geometry the coefficient of friction on faults is retrieved from the distribution of the P -axis azimuths (Iio 1997). The focal mechanisms having P -axis plunges less than 60° was used to constitute the frequency distribution of the P -axis azimuths. The width of the frequency groups, i.e., the bins were set at 10° . According to

Table 1 Source parameters obtained through CMT inversion results of the events in eastern Marmara region

No	Date	Time	Latitude	Longitude	M_w	CMT depth	Strike	Dip	Rake
1	June 23, 2002	23:09	40.76	29.03	2.7	3	340	66	-78
2	July 22, 2003	23:55	40.73	29.07	3.0	2	110	45	-137
3	May 16, 2004	03:30	40.70	29.33	4.3	10	89	69	-124
4	May 16, 2004	21:07	40.70	29.31	3.3	5	100	48	-128
5	September 29, 2004	15:42	40.79	29.02	4.0	13	88	67	82
6	September 29, 2004	15:51	40.78	29.04	2.7	20	291	57	-163
7	August 14, 2005	21:11	40.74	29.04	3.4	4	315	58	-97
8	September 7, 2005	13:22	40.73	29.22	3.3	9	281	70	-135
9	September 7, 2005	13:50	40.74	29.25	3.2	9	290	48	-127
10	November 26, 2005	22:27	40.65	29.07	3.2	6	292	56	-109
11	October 28, 2006	15:28	40.64	29.23	3.2	3	222	85	-149
12	March 12, 2008	18:53	40.62	29.01	4.8	10	89	78	-129
13	August 18, 2008	11:06	40.71	29.12	3.0	12	248	56	-175
14	August 18, 2008	11:08	40.72	29.12	3.1	10	265	64	-160
15	October 5, 2008	06:04	40.63	29.01	4.2	15	89	51	-117
16	October 22, 2008	01:00	40.74	29.17	3.8	8	11	66	-22
17	February 21, 2009	22:29	40.76	29.05	3.3	6	303	53	-112
18	February 21, 2009	23:04	40.73	29.02	3.4	6	294	63	-111
19	July 12, 2009	06:59	40.67	29.17	3.3	8	253	36	-120
20	November 16, 2009	18:47	40.60	29.01	3.2	12	88	41	-140
21	May 9, 2011	03:01	40.85	29.29	3.3	6	277	60	-131
22	March 14, 2012	09:25	40.81	28.79	3.7	10	347	49	-124
23	September 24, 2012	09:24	40.81	28.79	4.4	15	160	20	-96
24	August 3, 2014	10:42	40.61	29.16	3.6	3	109	41	-70
25	August 3, 2014	22:22	40.61	29.17	4.1	12	118	43	-62

the Iio (1997) formulation portrayed in Fig. 5, when the pick of the normal distribution of the P -axis approaches the azimuth of σ_1 low values of μ should be expected and vice versa larger deviation of the P -axes from σ_1 requires higher values of μ .

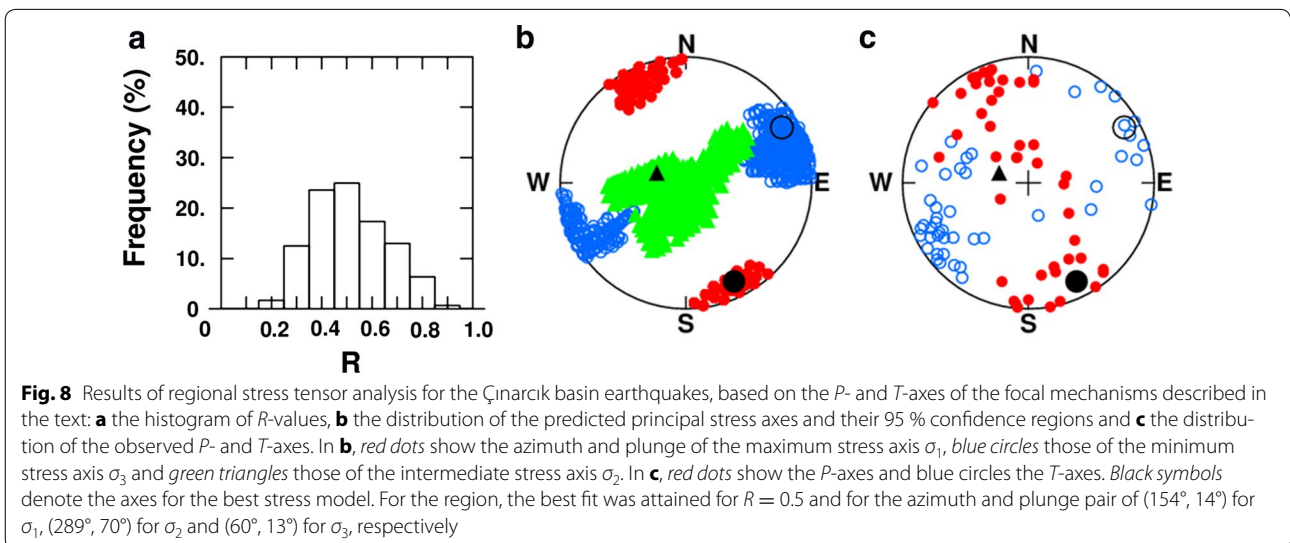
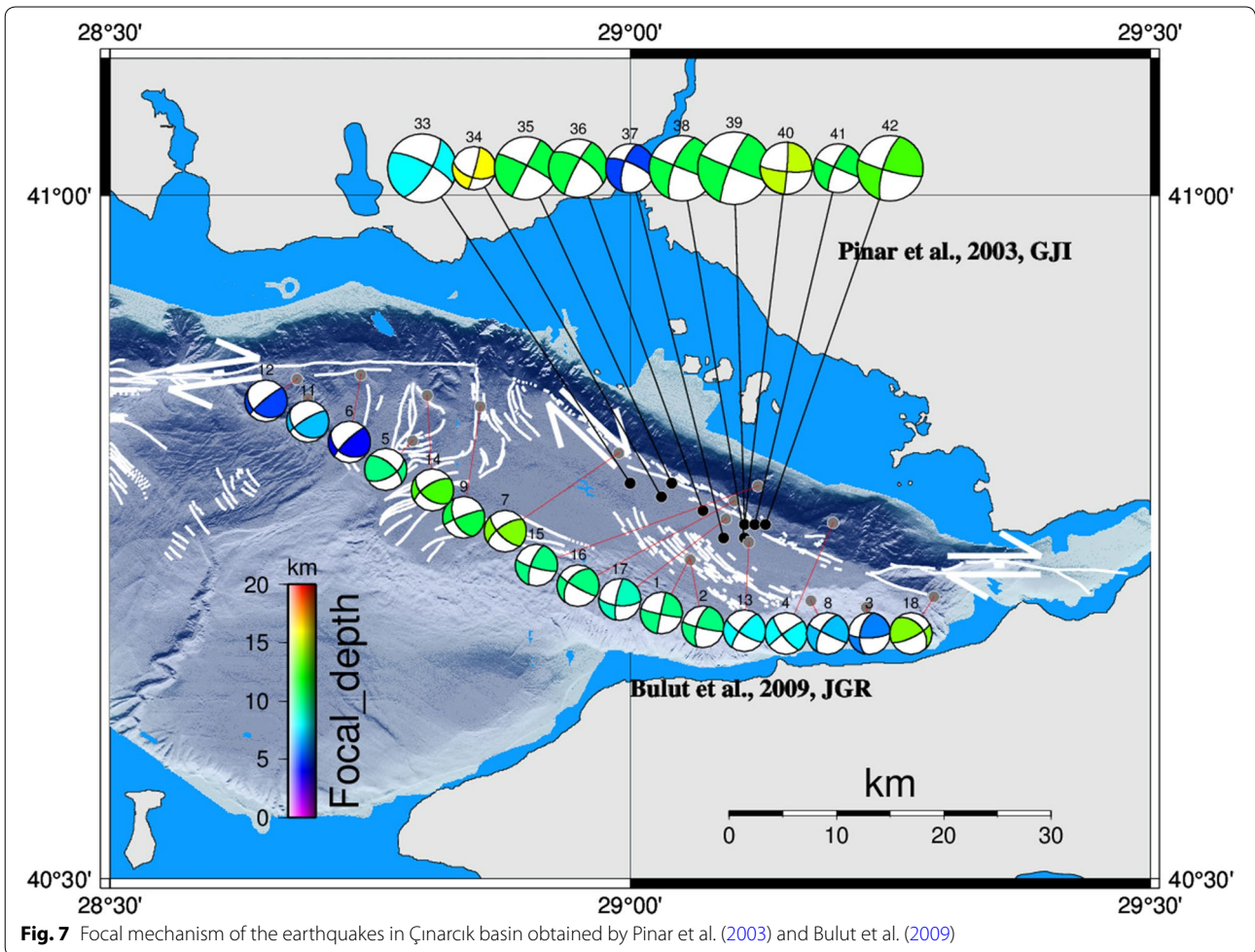
The frequency distribution of the P -axis of the 46 events shows a single peak around the azimuth of 150° (Fig. 9). Iio (1997) shows that for smaller μ values, the P -axis azimuth distribution has a narrow peak around the direction of the maximum compressional stress. In our estimations, the frequency distribution of the P -axes of the events showing a dominating peak at azimuth of 150° is close to the azimuth of σ_1 derived from the Çınarcık basin focal mechanisms. A comparison of the frequency distribution of the P -axis azimuths with a calculated normal distribution curve for a value of $\mu = 0.1$ with standard deviation of 10 is shown in Fig. 9 where the solid line shows the observations and the dashed line is the calculations. The good fit between the observed and the theoretical normal distributions attained for $\mu = 0.1$ and 150° azimuth of σ_1 suggests a rather low frictional strength for the faults occurring in Çınarcık basin.

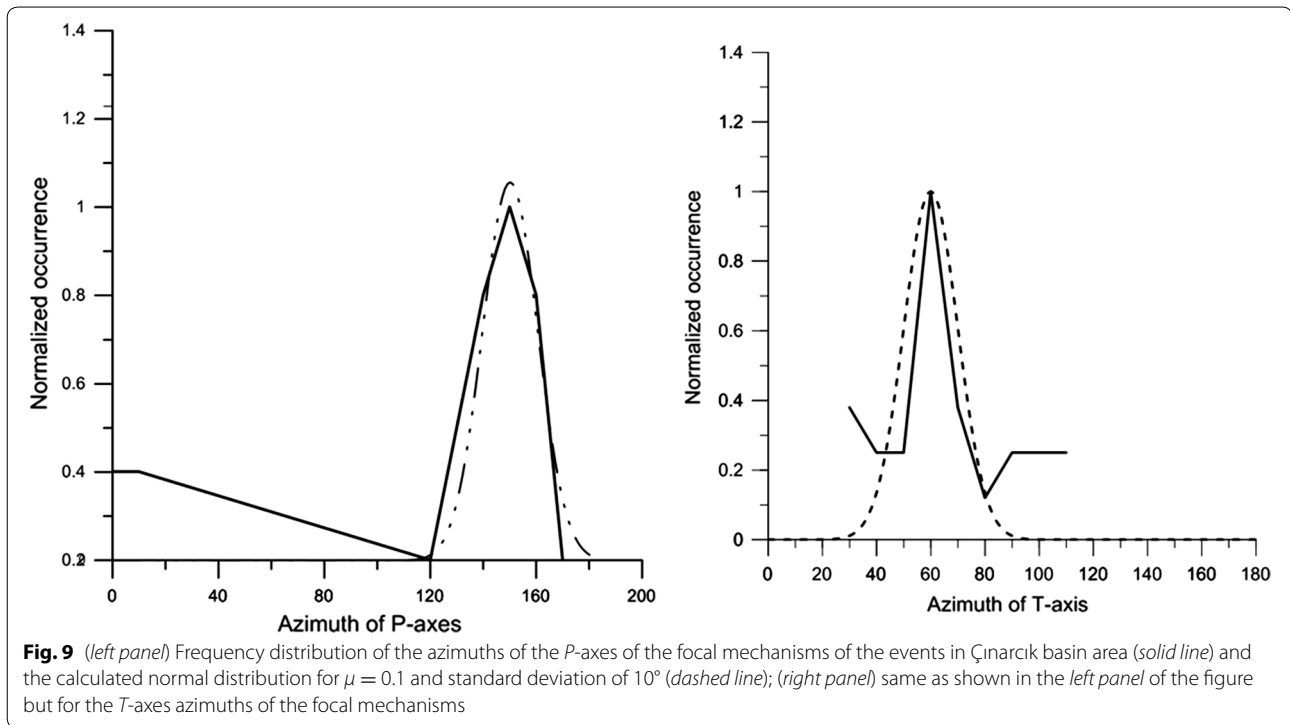
Similar analysis was carried out using the T -axes of the focal mechanisms. The frequency distribution of the T -axes indicates a peak around azimuth of 60° , which is orthogonal to the azimuth of σ_1 , i.e., close to the orientation of the minimum compressive σ_3 principal stress axis. Thus, our results portray a fact that for a case of low frictional fault strength the P -axis azimuths are close to the orientation of σ_1 (Fig. 9, left panel) while the T -axis azimuths are almost in line with the σ_3 principal stress axis (Fig. 9, right panel).

Frequency distribution of the azimuths of P - and T -axes in Yalova–Çınarcık area

The depth cross section of the hypocenters of the aftershocks around Yalova–Çınarcık area took place in a zone between 5 and 12.5 km (Ito et al. 2002). Using the first-motion polarity data of the aftershocks recorded at more than ten stations Pinar et al. (2010) determined simultaneously focal mechanisms of 111 aftershocks shown in Fig. 10 and a stress tensor using the method of Horiuchi et al. (1995).

They derived a principal maximum compressive stress axes oriented almost E–W where the azimuths of the P - and





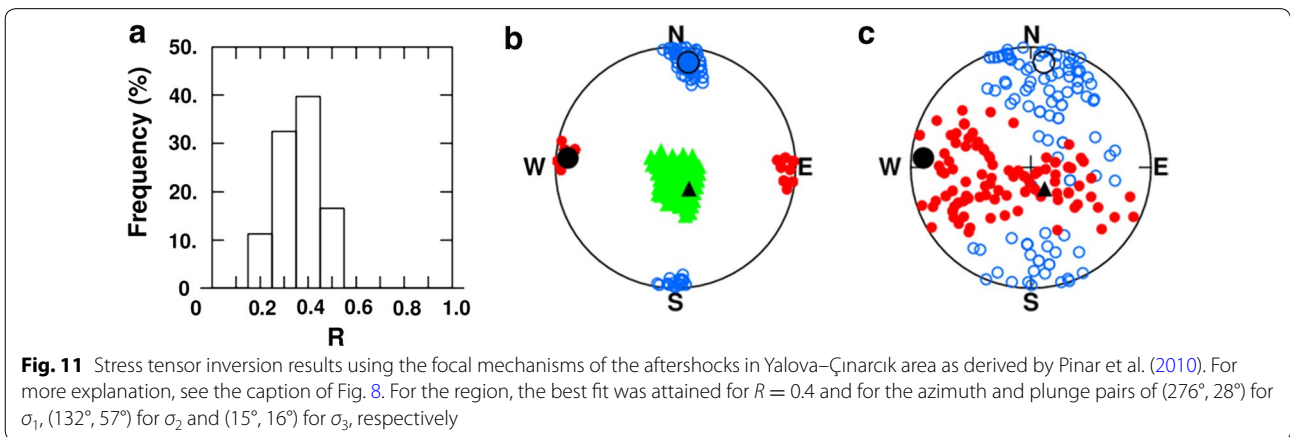
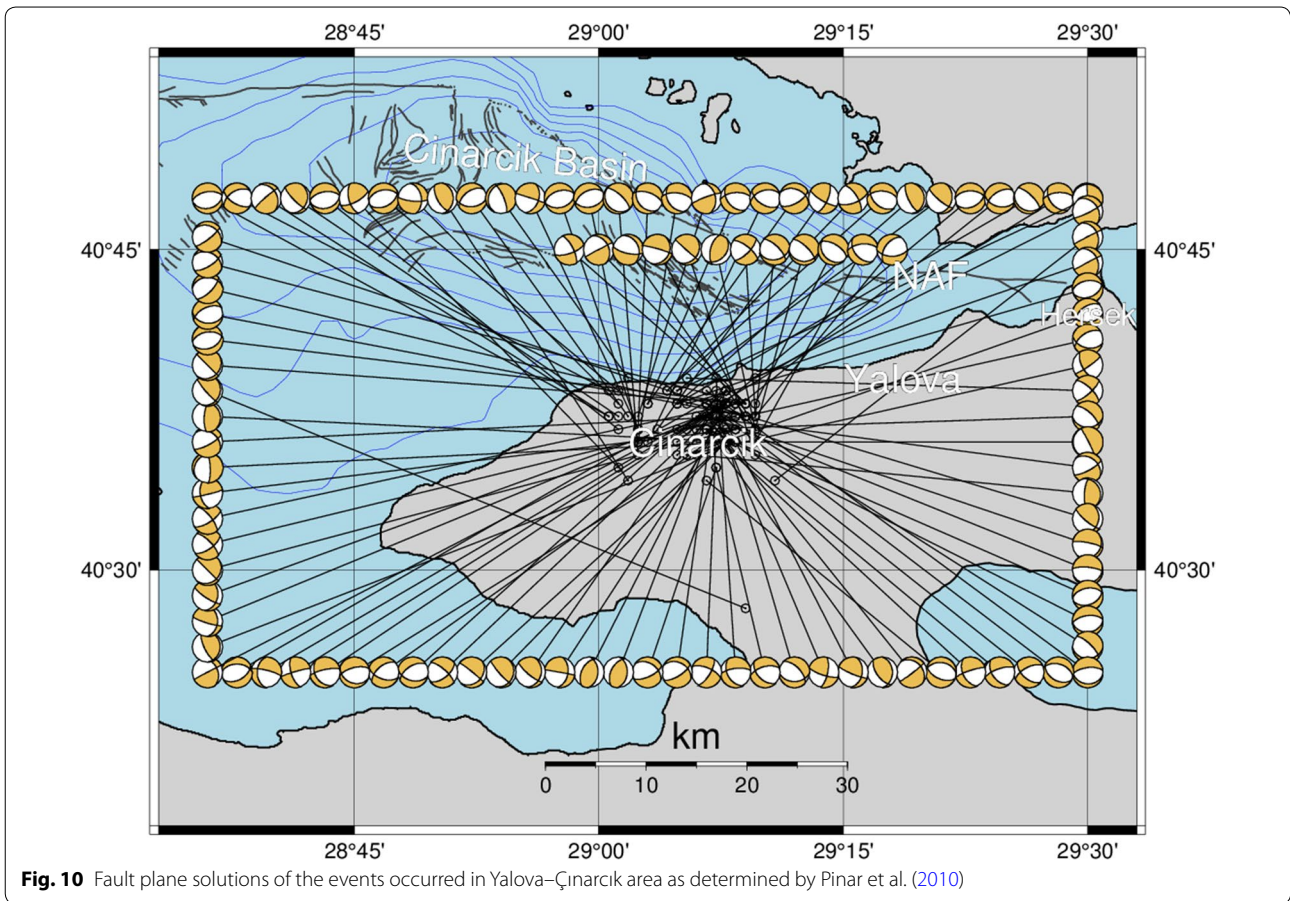
T -axes of the focal mechanisms were mostly E–W and N–S, respectively. The lower hemisphere projections of the P -axes show an E–W alignment parallel to the trend of the NAFZ, while the T -axes are oriented in direction normal to the NAFZ. The results obtained by Pinar et al. (2010) shows azimuth and plunge pair of the best maximum compressive stress axis (σ_1) as 268° and 46° , respectively. The plunge of the minimum compressive stress axis being close to horizontal (15°) points out a trans-tensional stress regime.

Pinar et al. (2010) yield P -axis plunges widely distributed in horizontal to vertical directions, while those of T -axes are concentrated in a narrower range. The aim of frictional strength analyses is to estimate the difference between the direction of the maximum compressional stress and fault plane; thus, it is not necessarily to analyze only P -axes since the T -axis also carries similar information about the fault plane. If the magnitudes of the maximum and intermediate compressional stresses are close, it is possible that directions of P -axes are widely distributed because this distribution does reflect not only frictional strength, but also the differences in the stress magnitudes.

Taking into account the above-mentioned facts, we retrieved a stress tensor using the 111 focal mechanisms of Pinar et al. (2010) and the stress tensor inversion method of Gephart (1990). The stress tensor inversion results yield nearly E–W maximum compressive stress axis similar to the orientation of σ_1 derived by Pinar et al.

(2010) but closer to horizontal (Fig. 11b). Significant number of the stress tensors fitting the observed focal mechanisms within 95 % of confidence interval yields a stress magnitude ratio (R) smaller than 0.5 (Fig. 11a). By definition, such values of R point out stress magnitudes of σ_1 and σ_2 getting closer to each other that might be the causative for the P -axis plunges being distributed from horizontal to vertical directions (Fig. 11c).

Figure 11c illustrates the azimuth and plunge of the P - and T -axes of the focal mechanisms where the scattering of the P -axes is larger than the T -axis. The results in Fig. 8 indicate that the frictional strength analyses based on the estimation of the differences between the direction of the maximum compressional stress and the fault plane geometries can be derived not only from the P -axes azimuths but also from the T -axis. In this respect, we construct frequency distribution curves for both the P - and T -axis azimuths of the focal mechanism shown in Fig. 9. The frequency distributions of the P - and T -axes azimuths of the Yalova–Çınarcık events are quite different from the frequency distributions of the Çınarcık basin events possessing one minimum and two maximums (Fig. 12). The two minimums of the P - and T -axis distributions are close to the orientations of the σ_1 and σ_3 principal stress axes, respectively, illustrated in Fig. 11b, while the peaks are about 30° away from the minimums. The best fit between the observed and the calculated distributions are achieved for frictional strength of $\mu = 0.8$

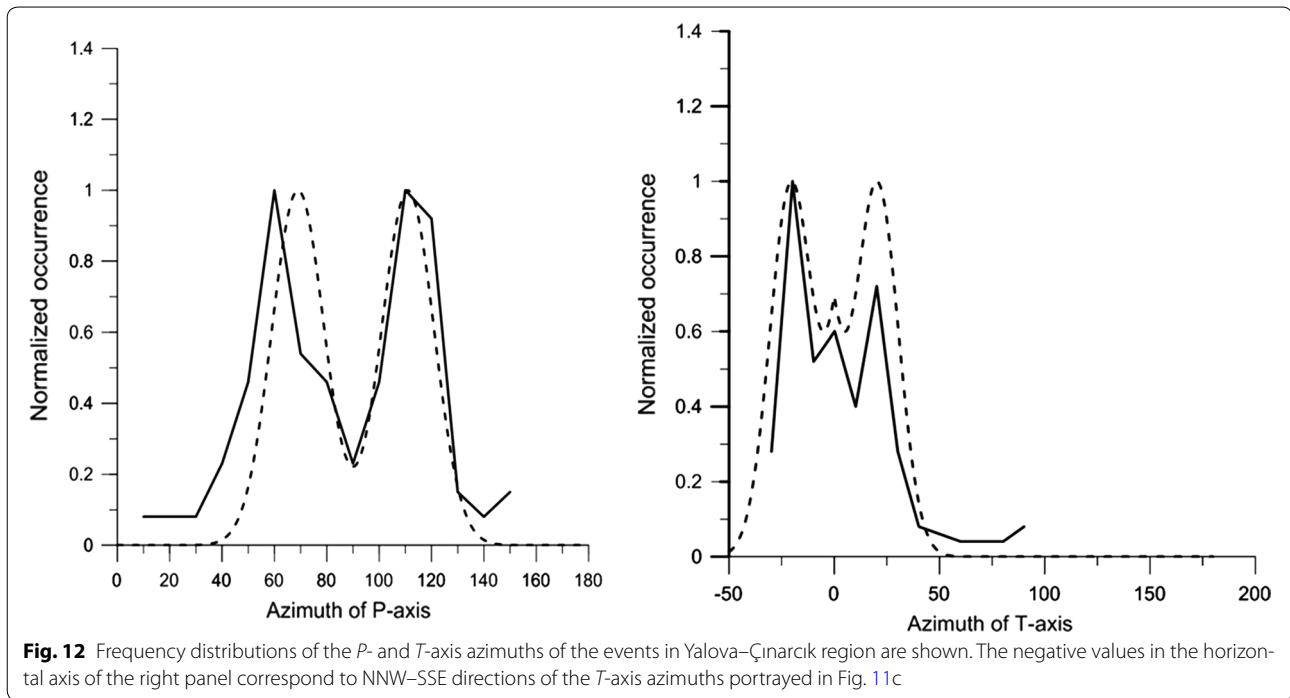


corresponding to a rather strong fault between Yalova and Çınarcık.

Frequency distribution of the azimuth of P - and T -axes in Yalova–Hersek area

For the area between Yalova and Hersek, 68 aftershocks were recorded at 10 stations or more providing 729

first-motion P -wave polarity data that were used for stress tensor inversion by Pinar et al. (2010). Their inversion results yield maximum and intermediate principal stress axes close to horizontal and minimum compressive stress axis far from horizontal, suggesting a transpressive tectonic stress regime in the western part of the Gulf of Izmit. The focal mechanism retrieved from the events



in Yalova–Hersek area is portrayed in Fig. 13, where strike-slip and thrust events are dominating. Having *P*-axis plunge values larger than 60° , we have discarded 4 focal mechanism solutions out of 68 events from further analysis. The rest of the events are classified as 38 strike-slip and 26 thrust events taking into account the *T*-axis plunge values being smaller and larger than 45° , respectively (Fig. 13).

The *P*- and *T*-axes of the focal mechanisms in Fig. 13 are then used to estimate a local stress tensor acting in Yalova–Hersek area using the inversion method given in Gephart (1990). The results of the stress tensor inversion are given in Fig. 14b showing a σ_1 maximum compressive stress axis having orientation similar to the regional stress tensor in Marmara region prior to 1999 İzmit earthquake (Pinar et al. 2010). Figure 14a shows that a significant number of the stress tensors fitting the observed focal mechanisms within 95 % of confidence interval yield a stress magnitude ratio, R , between 0.0 and 0.4. As was pointed out such values of R reflect stress magnitudes of σ_1 and σ_2 being close to each other which in turn explains the widespread distribution of the *P*- and *T*-axis plunges distributed from horizontal to vertical directions (Fig. 14c).

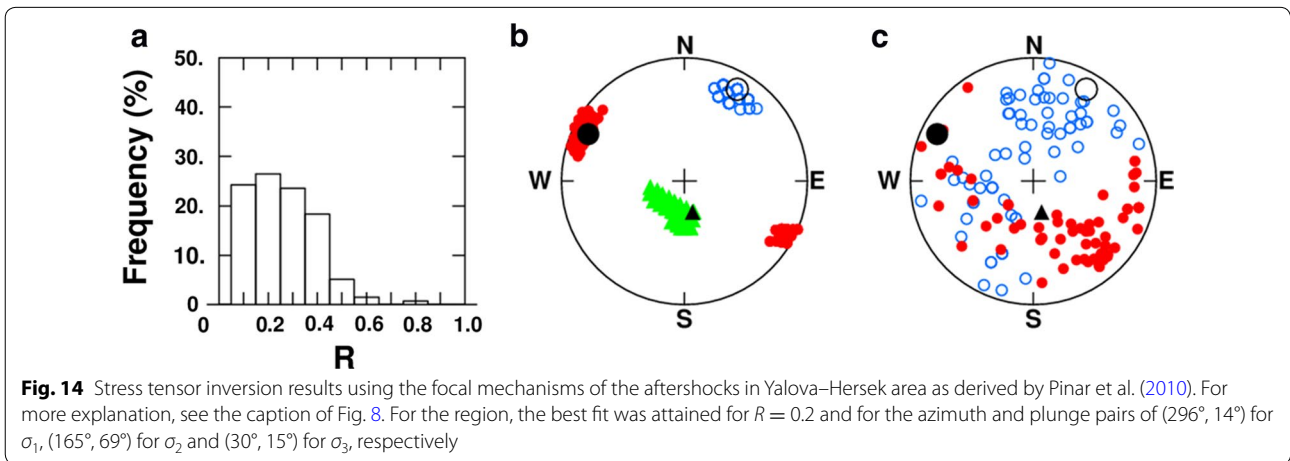
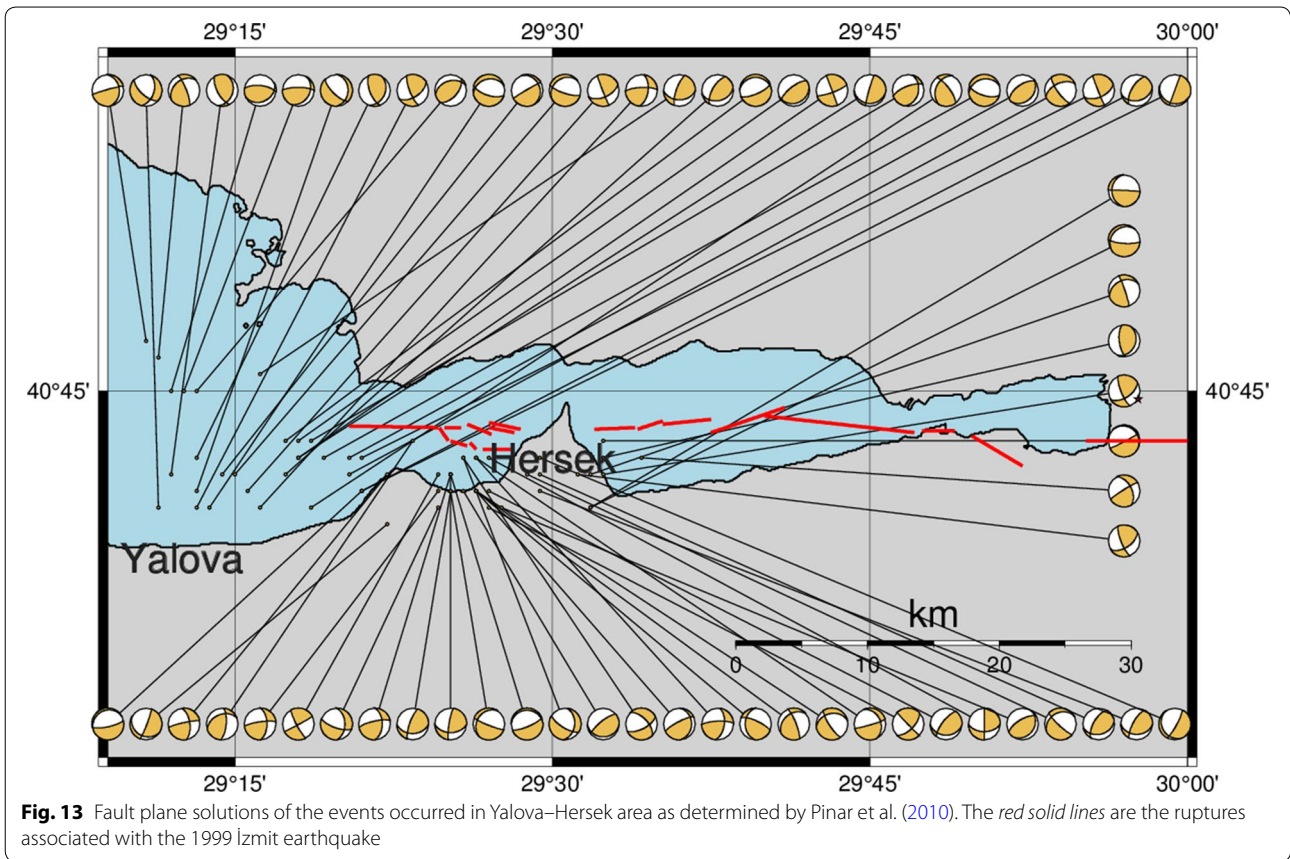
We will investigate the frictional strength of the faults in Yalova–Hersek area through a comparison of the maximum compressive stress axis azimuth and the strike of the fault planes. In this frame, we will handle the strike-slip and thrust events separately. The frequency

distribution of the azimuths of the *P*-axis of the strike-slip events has a minimum close to the σ_1 azimuth (N120°E) and two maximums at about 15° away from the minimum at about 105° and 135° (Fig. 15). The modeling of such observed frequency distribution yields a high frictional strength for the strike-slip faults achieved at calculation for $\mu = 0.6$ (Fig. 15).

On the other hand, Iio (1997) shows that a similar analysis can be done using the *P*-axis plunges of the thrust events since they correspond to the *P*-axis of the strike-slip events. The plunge of the maximum compressional stress shown in Fig. 14b is almost horizontal. Thus, if the faults were weak in the region then the *P*-axis plunges should be distributed around 0° . However, a rose diagram in Fig. 16 showing the frequency distribution of the *P*-axis azimuths (left) and plunges of the thrusting events (right) supports the fact of a strong frictional fault strength, as was derived from the strike-slip faults (Fig. 15). Here, the maximum frequency of the *P*-axis azimuths is around 315° – 320° (Fig. 16, left) which is about 15° – 20° away from the azimuth of the maximum compressive stress axis in Fig. 14b. Likewise, the plunges of the *P*-axis are in average about 15° away from the plunge of the maximum compressive stress axis (Fig. 16, right).

Discussion and conclusions

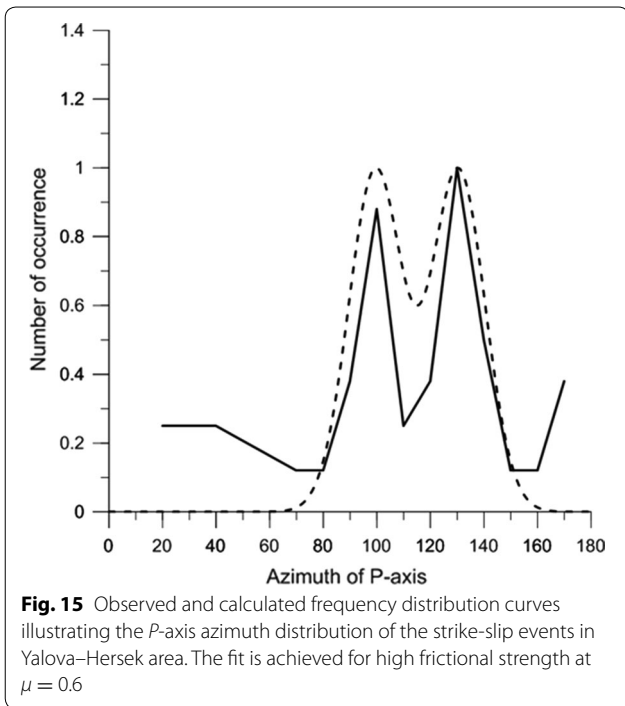
The stress tensor inversion using the focal mechanisms of large events occurred in the last century in Marmara region has shown predominantly strike-slip regime with



maximum compressive principle stress axis oriented approximately with an azimuth of about 300° (Kıratzi 2002; Pinar et al. 2010; Örgülü 2011). Most of these large events ruptured several segments of NAF zone.

The fault segment of NAF in the Çınarcık basin named as Princes’ Island fault segment cuts the deep sediments of the basin from SE to NW direction where it connects with the

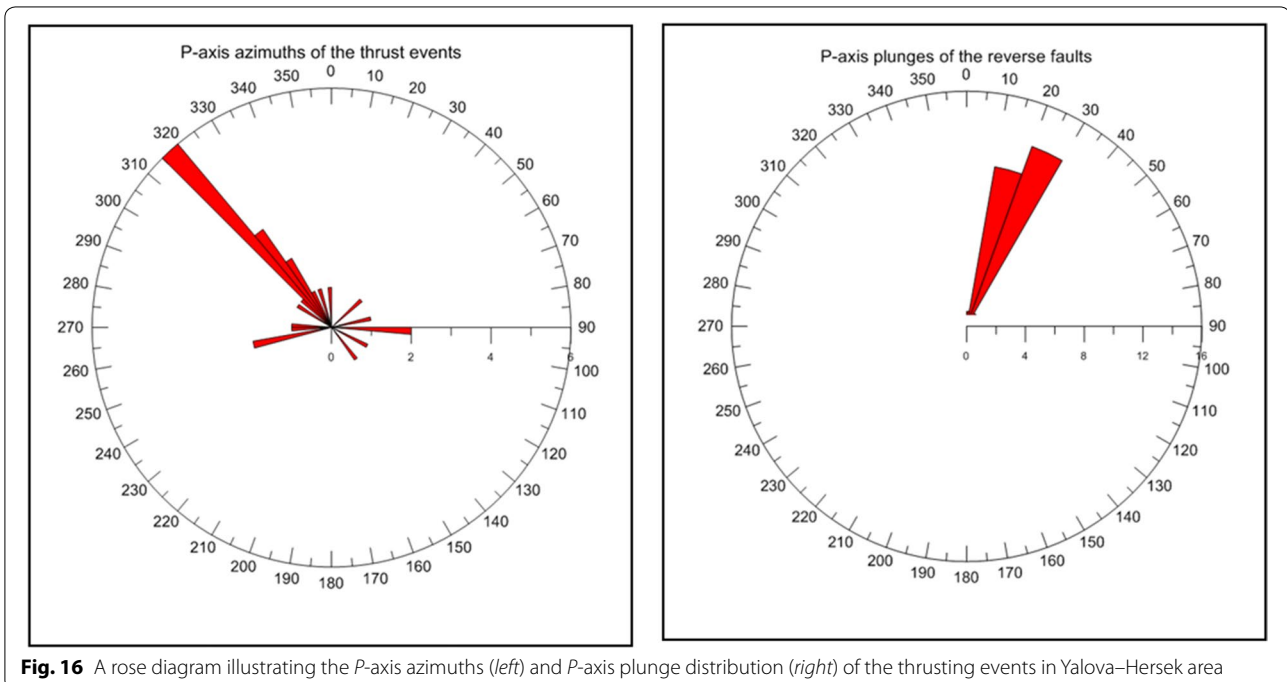
main Marmara fault segment. To the east of the basin, the Yalova–Hersek segment of NAF goes through the Gulf of İzmit extending between Çınarcık basin and Hersek delta (Okyar et al. 2008). Thus, the Princes’ Islands and the Yalova–Hersek segments are on-fault segments following the main trace of NAF zone in eastern Marmara Sea region, while the Yalova–Çınarcık segment is an off-fault segment (Fig. 1).



Several fault plane solutions of small size earthquakes around these fault segments exist. Based on those focal mechanisms, the geometry of the maximum principal stress axis and the fault orientations provide evidence on the frictional strength of NAF zone where our

analysis results point out low frictional fault strength along Çınarcık basin segment. On the other hand, the Yalova–Çınarcık fault is an off-fault segment laying to the south of the main NAF trace on the Armutlu peninsula where we obtained high frictional strength. Similar fault strength property was determined from the focal mechanisms around Yalova–Hersek segment. The low frictional strength derived from the events along the Princes Islands fault zone suggest that the North Anatolian fault crossing the Çınarcık basin is a weak crustal fault zone compared with the surrounding rocks. The San Andreas fault (SAF) zone and the North Anatolian fault zone possess quite similar features in fault length, slip rate and seismic behavior. Our results from the Çınarcık basin portray another feature of similarity of SAF and NAF, i.e., existence of low frictional strength portions along the two large transform faults (Carpenter et al. 2011).

Evidences on low frictional strength of NAF zone in eastern Marmara Sea region was also reported by Ergintav et al. (2007) using GPS data. The GPS network operated in Marmara region was used to construct a profile crossing the NAF zone in eastern Marmara Sea region with the aim to capture the slip rate variations along the profile. The modeling of the GPS profile crossing a region close to the Princes’ Island segment reveals shallow locking depth of about 3 km. The causatives for the observed profile might be either the shallow locking depth or low frictional strength. According to Ergintav et al. (2007) the ongoing post-seismic slip following the 1999 İzmit



earthquake ($M_w = 7.4$) could also generate such results. But, there is a long lasting debate on whether the western termination of the 1999 İzmit earthquake crossed Hersek Delta where contradicting claims exists (e.g., Uçarkuş et al. 2011 and references therein).

Most of the focal mechanisms of the events around Yalova–Çınarcık and Yalova–Hersek segment belong to the period when the so-called post-seismic slip was underway; therefore, the high fictional strength along the Yalova–Hersek and Yalova–Çınarcık segments provides an alternative view on the ongoing discussions. Although the GPS profile modeling of Ergintav et al. (2007) supports the low frictional fault strength in Çınarcık basin, it seems to contradict with the high frictional results we determined for Yalova–Hersek and Yalova–Çınarcık sites.

However, those GPS results are somewhat questionable. One can notice from the GPS paper that these contradicting results include two GPS stations (OLUK and YANT, Figs. 3 and 5 of Ergintav et al. 2007) which are 40–45 km apart from each other, though both of them are located very close to the NAF fault trace; OLUK is located on the Anatolian block to the east of Hersek delta, while YANT is located on the Eurasian block close to the Princes' islands. Another contrasting point of this pair of stations is that large co-seismic fault displacements were measured nearby OLUK station associated with the 1999 İzmit earthquake, while the Princes' islands segment close to the YANT station was not ruptured at all. Thus, although the YANT station is on the northern block of NAF and the OLUK station on the southern block of NAF, by virtue of the fact that these two locations are far from each other they should not be combined in constructing a common GPS profile. Probably, because of these reasons there is no obvious correlation between our findings and the GPS results in eastern Marmara region.

It is noteworthy to state that the width of the GPS profile spans the whole rupture zone of the 1999 İzmit earthquake; therefore, its resolution should not be expected to be high enough to distinguish the different properties of the segments we observe. Thus, our results suggest no significant post-seismic slipping on the segments to the west of the Hersek Delta. Probably, the seismic activity on those segments was triggered by the static stress increase caused by the ruptures of the segments located to the east of the Hersek Delta (Pinar et al. 2001).

Such stress transfer could be the causative for the heterogeneity in the stress field to the west of Hersek. In Yalova–Çınarcık area, the P -axes oriented E–W are in parallel with the maximum compressive stress axis, while the T -axes oriented N–S are close to the orientation of the minimum principle compressive stress (Fig. 11). The

T -axis plunges of most of the events are close to horizontal, while the P -axis plunges are scattered between horizontal and vertical. When the T -axes are horizontal, the horizontal and vertical P -axis plunges reflect strike-slip and normal faulting mechanisms, respectively. This implies that the magnitudes of the vertical stress and the maximum horizontal stress in E–W directions are close. On the contrary, in Yalova–Hersek area the T -axis plunges are scattered in-between horizontal and vertical planes, suggesting that the magnitude of the vertical stresses are closer to the minimum horizontal stress magnitudes.

Also, considering the distance of the Princes Islands segment to the so-called western rupture termination (Fig. 13) of the 1999 İzmit earthquake and the fact that most of the focal mechanism data were recorded long time after the 1999 İzmit mainshock ($M_w = 7.4$) reduces the possibility of post-seismic slip to be the causative for the observed low frictional strength in Çınarcık basin area. Thus, we note that the possibility of a post-seismic slip to be the causative of the observed low frictional strength along the Princes Islands segment is rather low.

Moreover, the 2D resistivity images constructed from the OBEM (ocean bottom electro-magnetic) measurements and seismic tomography images derived in eastern Marmara region provide evidences on the weakness of the NAF zone along the Yalova–Çınarcık, Yalova–Hersek and the Princes' Island segments (Denli et al. 2010; Kaya et al. 2013). Although these results support the low fault strength idea in the Çınarcık basin, they contradict with the results for the other two segments. The 2D tomograms constructed from the first arrivals at local seismic stations in eastern Marmara region show low seismic velocity estimation for the blocks laying along the main trace of the NAF compared to the blocks surrounding the NAF zone (Denli et al. 2010). The assessment of the long-period OBEM records acquired at six locations along a profile crossing the Çınarcık basin revealed the existence of a conductor extending in depth range between the upper crust and the upper mantle. According to Kaya et al. (2013), a causative for the observed conductor could be the fluids in the crust and the partial melting in the upper mantle. In this study, we should note that most of the CMT locations retrieved from the Çınarcık basin earthquakes and Pinar et al. (2003) coincide with the depth range of the conductor (Table 1; Fig. 6).

The maximum compressive stress direction of the regional stress tensor ($\approx 300^\circ$) in Marmara region and the direction of σ_1 of the three local stress tensors derived from the events in Çınarcık basin ($\approx 330^\circ$), Yalova–Çınarcık fault zone ($\approx 270^\circ$) and the Yalova–Hersek zone ($\approx 300^\circ$) constitute quite interesting results. These results indicate that while the local stress field around

Yalova–Hersek segment is in line with the regional stress field, clockwise rotation of about 30° in Çınarcık basin and about 30° counterclockwise rotation in the local stress field around Yalova–Çınarcık segment is observed. The clockwise rotation develops in the blocks to the north of the E–W trending NAF, while the counterclockwise rotation occurs within the southern blocks. The observed rotation of the stress fields, i.e., the block rotations happens at the region coinciding with the conductor area proposed by Kaya et al. (2013) though it is hard to provide direct evidence for such a causative of stress rotation.

The geodynamical context of the clockwise and counterclockwise rotations can be examined with a model similar to the triple junction model of Okay et al. (2000) where the E–W trending NAF bifurcates in NW and SE trending branches in eastern Marmara Sea region (Fig. 1). According to the model of Okay et al. (2000), the Çınarcık basin started to form when the westward-propagating North Anatolian fault intersected a northwesterly trending preexisting fault zone during the Pliocene and bifurcated into NW- and SW-trending segments, forming a transform–transform–transform-type triple junction. Dextral strike-slip movement along the arms of the triple junction led to the development of the Çınarcık basin.

Authors' contributions

AP and ZC drafted the manuscript and performed the analysis. Both AP and ZC plotted the figures and wrote the final version. AM and DK contributed on data analysis and discussions. All authors read and approved the final manuscript.

Acknowledgements

This research was supported by Bogaziçi University Research Fund project code BAP9802D. The waveform data used for CMT inversion were obtained from KOERI seismic network (doi:10.7914/SN/KO). We appreciate the comments raised by the reviewers, the handling Editor Takane Hori and the chief editor Yasuo Ogawa who significantly improved the manuscript.

Competing interests

The authors declare that they have no competing interests.

Received: 30 July 2015 Accepted: 4 April 2016

Published online: 23 April 2016

References

- Ambraseys N (2002) The seismic activity of the Marmara Sea region over the last 2000 years. *Bull Seism Soc Am* 92:1–18
- Armijo R, Meyer B, Hubert-Ferrari A, Barka A (1999) Westward propagation of North Anatolian fault into the Northern Aegean: timing and kinematics. *Geology* 27:267–270
- Armijo R, Meyer B, Navarro S, King G, Barka A (2002) Asymmetric slip partitioning in the Sea of Marmara pull apart: a clue to propagation processes of the North Anatolian fault. *Terra Nova* 14:80–86
- Armijo R et al (2005) Submarine fault scarps in the Sea of Marmara pull apart (North Anatolian fault): implications for seismic hazard in Istanbul. *Geochim Geophys Geosyst* 6:Q06009. doi:10.1029/2004GC000896
- Barka A (2002) The 17 August 1999 Izmit earthquake. *Science* 285:1858–1859
- Becel A et al (2009) Moho, crustal architecture and deep deformation under the North Marmara Trough, from the SEISMARMARA Leg 1 offshore–onshore reflection–refraction survey. *Tectonophysics* 467:1–21
- Bulut FM, Bohnhoff M, Ellsworth W, Aktar M, Dresen G (2009) Microseismicity at the North Anatolian fault in the Sea of Marmara offshore Istanbul, NW Turkey. *J Res Geophys*. doi:10.1029/2008JB00624
- Carpenter BM, Marone C, Saffer DM (2011) Weakness of San Andreas Fault revealed by samples from the active fault zone. *Nat Geosci* 4:251–254. doi:10.1038/ngeo1089
- Carton H (2005) Etudes tectoniques en Mediterranee orientale par analyse dedonnees de sismique reflexion: Mer de Marmara Bassin de Çınarcık et merge du Liban, PhD thesis, Institute De Physique Du Globe De Paris
- Carton H et al (2007) Seismic imaging of the three-dimensional architecture of the Çınarcık Basin along the North Anatolian fault. *J Geophys Res* 112:B06101. doi:10.1029/2006JB004548
- Demirbağ E, Rangin C, Le Pichon X, Şengör AMC (2003) Investigation of the tectonics of the Main Marmara fault by means of deep-towed seismic data. *Tectonophysics* 361:1–19
- Denli A, Gürbüz C, Kissling EH (2010) Crustal velocity structure of eastern Marmara region from local earthquake tomography. American Geophysical Union Fall meeting 2010, abstract ED31C-0690
- Egeran N, ve Lahn E (1944) 1/2.400.000 Mikyaslı Türkiye Yer Depremleri Haritası Hakkında Muhtıra. *MTA Mec* 9(2/32):270–289
- Ergintav S, Dogan U, Gerstenecker C, Cakmak R, Belgen A, Demirel H, Aydın C, Reilinger R (2007) A snapshot (2003–2005) of the 3D postseismic deformation for the 1999, Mw = 7.4 Izmit earthquake in the Marmara region, Turkey, by first results of joint gravity and GPS monitoring. *J Geodyn* 44:1–18. doi:10.1016/j.jog.2006.12.005
- Gazioğlu C, Gökaşan E, Algan O, Yücel Z, Tok B, Doğan E (2002) Morphologic features of the Marmara Sea from multi-beam data. *Mar Geol* 190:397–420
- Gephart JW (1990) FMSI: a Fortran program for inverting fault/slickenside and earthquake focal mechanism data to obtain the regional stress tensor. *Comput Geosci* 16:953–989
- Gürbüz C, Aktar M, Eyidoğan H, Cisternas A, Haessler H et al (2000) The seismotectonics of the Marmara region (Turkey): results from a macroseismic experiment. *Tectonophysics* 316:1–17
- Horiuchi S, Rocco G, Hasegawa A (1995) Discrimination of fault planes from auxiliary planes based on simultaneous determination of stress tensor and a large number of fault plane solutions. *J Geophys Res* 100(5):8327–8338
- Ilio Y (1997) Frictional coefficient on faults in a seismogenic region inferred from earthquake mechanism solutions. *J Geophys Res* 102:5403–5412
- İmren C, Le Pichon X, Rangin C, Demirbağ E, Ecevitoglu B, Görür N (2001) The North Anatolian fault within the Sea of Marmara: a new interpretation based on multi-channel seismic and multi-beam bathymetry data. *Earth Planet Sci Lett* 186:143–158
- Ito A, Üçer SB, Barış Ş, Honkura Y, Nakamura A, Kono T, Pektaş R, Komut T, Hasegawa A, Işıkara AM (2002) Aftershock activity of 1999 Izmit earthquake, Turkey, revealed from microearthquake observations. *Bull Seismol Soc Am* 92:418–427
- Kalafat D, Gürbüz C, Üçer SB (1987) Batı Türkiyede kabuk ve üst manto yapısının araştırılması. *Deprem Araştırma Bülteni* 14:43–64
- Karabulut H, Bouin M-P, Bouchon M, Dietrich M, Cornou C, Aktar M (2002) The seismicity in the eastern Marmara Sea after the 17 August 1999 Izmit earthquake. *Bull Seismol Soc Am* 92:387–393
- Kaya T, Kasaya T, Tank SB, Ogawa Y, Tunçer MK, Oshiman N, Honkura Y, Matsushima M (2013) Electrical characterization of the North Anatolian fault zone underneath the Marmara Sea, Turkey by ocean bottom magnetotellurics. *Geophys J Int* 193:664–677. doi:10.1093/gji/ggt025
- Ketin İ (1948) Über die tektonisch-mechanischen Folgerungen aus den grossen anatolischen Erdbeben des letzten Dezenniums. *Geol Rund* 36:77–83
- Ketin İ (1968) Relations between general tectonic features and the main earthquake regions in Turkey. *Bull Miner Res Explor Inst Turk* 71:63–67
- Ketin İ, Rösl F (1953) Makroseismische Untersuchungen über das nordwest-anatolische Beben vom 18 März 1953. *Eclogae Geol Helv* 46:187–208
- King GCP, Stein RS, Lin J (1994) Static stress changes and triggering of earthquakes. *Bull Seismol Soc Am* 84:935–953

- Kiratzi A (2002) Stress tensor inversion along the westernmost North Anatolian fault zone and its continuation into the North Aegean Sea. *Geophys J Int* 151:360–376
- Kohketsu K (1985) The extended reflectivity method for synthetic near-field seismograms. *J Phys Earth* 33:121–131
- Kuge K (2003) Source modeling using strong-motion waveforms: toward automated determination of earthquake fault planes and moment-release distributions. *Bull Seismol Soc Am* 93:639–654
- Laigle M, Bécel A, de Voogd B, Hirn A, Taymaz T, Ozalaybey S, the Members of the SEISMARMARA Leg1 (2008) A first deep seismic survey in the Sea of Marmara: whole crust and deep basins. *Earth Planet Sci Lett* 270:168–179
- Le Pichon X, Taymaz T, Şengör AMC (1999) The Marmara fault and the future Istanbul earthquake. In: Proceedings of ITU-IAHS, international conference on the Kocaeli earthquake 17 August 1999, İstanbul, Turkey, 1999 December 2–5, pp 41–54
- Le Pichon X, Taymaz T, Şengör AMC, (2000) Important problems to be solved in the Sea of Marmara (NW-Turkey). In: NATO advanced research seminar: integration of earth sciences research on the 1999 Turkish and Greek earthquakes and needs for future cooperative research, İstanbul, Turkey, May 14–17, 2000. Abstract Book: pp 66–67
- Le Pichon X, Şengör AMC, Demirbağ E, Rangin C, İmren C et al (2001) The active main Marmara Fault. *Earth Planet Sci Lett* 192:595–616
- Le Pichon X, Chamot-Rooke N, Rangin C, Şengör AMC (2003) The North Anatolian fault in the Sea of Marmara. *J Geophys Res* 108(B4):2179. doi:10.1029/2002JB001862
- McKenzie DP (1972) Active tectonics of the Mediterranean region. *Geophys J R Astron Soc* 30:109–185
- Okay A, Kaşlılar-Özcan A, İmren C, Boztepe-Güney A, Demirbağ E, Kuşçu İ (2000) Active faults and evolving strike-slip basins in the Marmara Sea, northwest Turkey: a multichannel seismic reflection study. *Tectonophysics* 321:189–218
- Okyar M, Pinar A, Tezcan D, Kamacı Z (2008) Late quaternary seismic stratigraphy and active faults of the Gulf of İzmit (NE Marmara Sea). *Mar Geophys Res* 29:89–107
- Örgülü G (2011) Seismicity source parameters for small-scale earthquakes along the splays of the North Anatolian fault (NAF) in the Marmara Sea. *Geophys J Int* 184:385–404
- Örgülü G, Aktar M (2001) Regional Moment Tensor Inversion for Strong Aftershocks of the August 17, 1999 İzmit Earthquake (M_w 7.4). *Geophys Res Lett* 28:371–374
- Över S, Yılmaz H, Pinar A, Özden S, Ünlügenç UC, Kamacı Z (2013) Plio-Quaternary stress state in the Burdur Basin, SW-Turkey. *Tectonophysics* 588:56–68
- Özalaybey S, Ergin M, Aktar M, Tapırdamaz C, Biiçmen F, Yörük A (2002) The 1999 İzmit earthquake sequence in Turkey: seismological and tectonic aspects. *Bull Seismol Soc Am* 92:376–386
- Parke JR et al (1999) Active faults in the Sea of Marmara, western Turkey, imaged by seismic reflection profiles. *Terra Nova* 11:223–227
- Pinar N (1943) Marmara denizi Havzasının Sismik Jeoloji ve Meteoroloji/ Géologie et Météorologie Sismique du Bassin de Mer Marmara. PhD thesis. Inst. Géol., Inst. Phys. Gén. Univ. İstanbul, Kenan Matbaası. 63 pp +1 foldout map
- Pinar A, Honkura Y, Kuge K (2001) Seismic activity triggered by the 1999 İzmit earthquake and its implications for the assessment of future seismic risk. *Geophys J Int* 146:1–7
- Pinar A, Honkura Y, Kuge K (2003) Moment tensor inversion of recent small to moderate sized earthquakes: implication for seismic hazard and active tectonics beneath the Sea of Marmara. *Geophys J Int* 152:1–13
- Pinar A et al (2010) Spatial variation of the stress field along the fault rupture zone of the 1999 İzmit Earthquake. *Earth Planets Space* 62:237–256
- Rangin C, Demirbağ E, İmren C, Crusson A (2001) Marine atlas of the sea of Marmara (Turkey). Ifremer, Plouzané
- Rangin C, Le Pichon X, Demirbağ E, İmren C (2004) Strain localization in the Sea of Marmara: propagation of the North Anatolian fault in a now inactive pull-apart. *Tectonics*. doi:10.1029/2002TC001437
- Reilinger RE et al (2000) Coseismic and postseismic fault slip for the 17 August 1999, $M = 7.5$, İzmit, Turkey, earthquake. *Science* 289:1519–1524
- Sato T, Kasahara J, Taymaz T, Ito M, Kamimura A, Hayakawa T, Tan O (2004) A study of microearthquake seismicity and focal mechanisms within the Sea of Marmara (NW Turkey) using ocean bottom seismometers (OBSs). *Tectonophysics* 391:303–314. doi:10.1016/j.tecto.2004.07.018
- Şengör A, Tüysüz O, İmren C, Sakiç M, Eyidoğan H, Görür N, Pichon XL, Rangin C (2005) The North Anatolian fault: a new look. *Annu Rev Earth Planet Sci* 33:37–112
- Smith A, Oktay F, Taymaz T, Jackson J, Başaran H, Alpar B, Şimşek M, Kara S (1995) High resolution of seismic profiling in the Sea of Marmara-NW Turkey: late quaternary sedimentation and sea-level changes. *GSA Bull* 197:923–936
- Stefanik M, Jurdy DM (1992) Stress observations and driving force models for the South American plate. *J Geophys Res* 97:11905–11913
- Stein RS, Barka AA, Dieterich JH (1997) Progressive failure on the North Anatolian fault since 1939 by earthquake stress triggering. *Geophys J Int* 128:594–604
- Taymaz T, Jackson J, McKenzie D (1991) Active tectonics of the north and central Aegean Sea. *Geophys J Int* 106:433–490
- Toksöz M, Şakal A, Michael A (1979) Space-time migration of earthquakes along the North Anatolian fault zone and seismic gaps. *Pure Appl Geophys* 117:1258–1270
- Twiss RJ, Moores EM (1992) Structural geology. Freeman, New York
- Uçarkuş G, Çakır Z, Armijo R (2011) Western termination of the M_w 7.4, 1999 İzmit earthquake rupture, implications for the expected large earthquake in the Sea of Marmara. *Turk J Earth Sci* 20:379–394. doi:10.3906/yer-0911-72
- Wong HK, Lüdmann T, Uluğ A, Görür N (1995) The Sea of Marmara: a plate boundary sea in an escape tectonic regime. *Tectonophysics* 244:231–250
- Zoback ML (1993) Utilizing in situ stress data for seismic hazard assessment: The World Stress Map Project's contribution to GSHAP. *Ann Geofis* 36:217–224
- Zoback MD et al (1987) New evidence on the state of stress of the San Andreas fault system. *Science* 238:1105–1111

Submit your manuscript to a SpringerOpen® journal and benefit from:

- Convenient online submission
- Rigorous peer review
- Immediate publication on acceptance
- Open access: articles freely available online
- High visibility within the field
- Retaining the copyright to your article

Submit your next manuscript at ► springeropen.com